SSRG International Journal of Mechanical Engineering
ISSN: 2348-8360/ https://doi.org/10.14445/23488360/IJME-V13I8P106

Volume 13 Issue 8, 57-66, August 2026

Original Article

Influence of Stress Amplitude and Loading Frequency on Fatigue Performance of AA2024 Alloy under Two Temper Conditions

J. Jagadesh Kumar[1], Udaya Sri Kakarla[2], Ganesh Vantepaka[3], P. V. Gopal Krishna[4], Vaddi Venkata Satyanarayana[5*]

[1, 3, 5]*Department of Mechanical Engineering, Vidya Jyothi Institute of Technology, Aziznagar, Hyderabad, India.*
[2]*Department of Mechanical Engineering, KG Reddy College of Engineering and Technology, Hyderabad, India.*
[4]*Department of Mechanical Engineering, Vasavi College of Engineering, Ibrahimbagh, Hyderabad, India.*

[5*]*Corresponding Author: vvs@vjit.ac.in*

Received: 27 May 2026 Revised: 24 July 2026 Accepted: 07 August 2026 Published: 27 August 2026

Abstract - *AA2024 aluminium alloy is commonly used in fatigue-sensitive aerospace structures, but the relative effects of temper condition, stress amplitude and loading frequency on its fatigue durability are not sufficiently quantified. The present work examines the fatigue performance of AA2024-T3 and AA2024-T6 using Taguchi L9 experimental design with maximum stress level and loading frequency as chosen factors at two levels. Fatigue tests were performed at a sinusoidal tension-to-zero loading followed by Taguchi-ANOM, ANOVA, regression modelling and SEM fractographic evaluation. The findings indicated that the average fatigue life decreased by about 44% in AA2024-T6 and 39% in AA2024-T3 by increasing stress levels from 320 to 340 MPa. All test conditions showed that AA2024-T3 performed better than AA2024-T6 by about 7-18%, which means that there is a more favourable fatigue response in T3 relative to T6 despite the traditional advantage of static strength of T6. ANOVA confirmed stress amplitude to be the primary factor, with 97.01% and 93.90% contribution to fatigue-life in T6 and T3, respectively. The percentage contribution of frequency was only 2.40 and 4.12 in T6 and T3, respectively. Regression models were found to be highly predictive, and the R^2 of both models was found to be 0.9979 and 0.9966, respectively, with the confirmation-test deviations of 5.07%-7.02%, respectively. The results determined AA2024-T3 as the most fatigue-resistant temper among the high-cycle regimes explored.*

Keywords - *A2024, Solution treatment, Stress amplitude, Loading frequency, Fatigue life.*

1. Introduction

The 2xxx series of aluminium alloys still remains as a popular choice for fatigue-sensitive structural systems due to their attractive combination of low density, high specific strength, fracture toughness and established processability.

AA2024 is one of the most commonly used wrought alloys in aerospace skins, stiffened panels, fuselage structures, wing components, and other parts that require mechanical performance where cyclic loading is inevitable. Its extended industrial applicability is not just a by-product of the statical strength alone; it is the consequence of the larger balance between weight saving, manufacturability, damage tolerance and service reliability. Monotonic yielding or ultimate failure is not the only design parameter in aircraft and transport structures, but also the cumulative damage of repeated loading of the material. This renders fatigue life as a decisive attribute in alloy selection, temper designation, inspection schedule and structural endurance evaluation [1-4].

The superior fatigue performance of AA2024 is due to its precipitation-hardened microstructure. This alloy is part of the Al-Cu-Mg system, and the mechanical behaviour is highly sensitive to the size, morphology, spatial distribution and stability of the strengthening precipitates, the associated dislocation substructure and the residual internal stresses [5].

The various temper conditions of the material do not merely alter tensile properties alone; they alter the way cyclic strain localizes, how persistent slip develops, where crack initiation occurs, and how short cracks transition into stable propagation. This is especially important in aerospace-grade aluminium alloys since the metallurgical state that optimises hardness or tensile strength is not necessarily the one that optimises fatigue resistance. A higher nominal strength temper can spread the cyclic deformation in a more uniform way and hence delay the onset of a crack, but a lower nominal strength temper can spread the cyclic deformation in a more uniform way and hence delay the onset of a crack. In the example of AA2024, the temper condition must, therefore, be viewed as a key design variable and not a second material description [5, 6].

A combination of microstructural heterogeneity and the intensity of cyclic loading controls the fatigue failure in AA2024. Past studies of alloy and very similar tempers have shown that fatigue damage is generated in a sequence (local strain accumulation by plastic deformation, crack initiation at constituent particles or microstructural discontinuities, short-crack growth under high local driving forces and eventual long-crack propagation to ultimate failure) [7-9]. Using crack-growth and fractographic studies, previous studies also found that the crack path of AA2024 is sensitive to the loading history, crystallographic orientation and local microstructural resistance. Hence, the fatigue life of the material cannot be explained by nominal values of stress alone [10, 11]. More recent studies on AA2024-T351 also reinforced this view by linking fatigue response to cyclic hardening behaviour, modulus degradation, and multiaxial damage evolution. The studies hence confirmed that fatigue performance is fundamentally microstructure-dependent and strongly path-sensitive [6, 12]. All these findings are indicative of the fact that any effort to enhance or rationalize fatigue resistance in AA2024 must take into consideration not only the magnitude of the applied load, but the metallurgical state in which such a load is experienced.

Among the external loading variables, stress amplitude is one of the most direct and influential factors controlling the material's fatigue life. Increasing stress amplitude intensifies cyclic plasticity, slip-band formation, and microcrack initiation, and reduces the number of cycles needed for crack formation and propagation. In aluminium alloys, the correlation is particularly high because even small variations in stress level can alter the deformation mode from largely elastic cycling to locally concentrated plasticity around the microstructural heterogeneities. Past studies on AA2024 have indicated that there is a high sensitivity to stress-life in both low-cycle and high-cycle regimes, with mechanisms of crack initiation and morphology of failure becoming increasingly severe with increasing stress amplitude [7, 8]. Even though the dominant role of stress amplitude is well established, its quantitative influence is not explored for different temperaments of AA2024. The same nominal stress may result in different fatigue responses in two metallurgical conditions if their precipitate structures, internal stresses, and cyclic hardening responses differ. This is one of the principal reasons why a temper-comparative fatigue study remains necessary.

Loading frequency is another practical factor worth considering. In many fatigue experiments, researchers fix the frequency at a convenient level to shorten test time and keep the machine stable. That makes sense from a testing standpoint, but it risks hiding the physical role of loading rate in fatigue damage. Frequency affects several damage processes, including local hysteresis heating, environmental activity at crack tips, time-dependent microstructural relaxation, and the balance between crack closure and crack growth. The size of this effect depends on the alloy, temperature, environment, and frequency range. For AA2024, the evidence is useful, but not fully consistent. Mayer et al. found no clear frequency effect between 8 and 10 Hz for AA2024-T351 under their test conditions, which suggests the effect is limited within a narrow, conventional servo-hydraulic range [13]. Broader mechanistic studies point in a different direction. They show that loading frequency still matters for fatigue initiation, hysteresis-related energy loss, and very-high-cycle fatigue response, even when stress amplitude remains the dominant factor in standard laboratory testing [14, 15]. For this reason, frequency should not be treated as a minor testing detail. This is especially true when the aim is to develop design guidance, rather than produce isolated S-N data points.

The current literature on AA2024 fatigue is substantial, but it remains fragmented in a way that leaves several practical questions unresolved. A large body of work has focused on single temper conditions, specific crack-growth regimes, welded or surface-modified states, temperature effects, multiaxial loading, or very-high-cycle behaviour. These studies are valuable because they illuminate individual mechanisms. Nevertheless, relatively fewer studies compare two temper conditions of the same alloy under an identical matrix of stress amplitudes and loading frequencies while keeping specimen geometry, surface condition, and test protocol consistent. This limitation matters because it is precisely such a side-by-side comparison that enables the temper effect to be isolated from the load effect. Without that structure, differences in fatigue life can be confounded by differing specimen sources, different test frequencies, or differing stress windows [5, 15]. For practicing engineers, this means that the available literature often provides mechanistic insight but less often delivers a compact decision framework for selecting between two temper conditions under a defined cyclic loading envelope.

The other problem is related to the manner in which the results of fatigue are usually reported. Traditional S-N curves are not all that, and in themselves do not always show the relative significance of various control factors. When multiple parameters affect the response at the same time, designers require more than descriptive tendencies; they require a ranking insight regarding which of the numerous parameters affects the observed variation and which of the numerous parameters merely fine-tunes the response. This is where the experimental design and statistical reduction come in handy. With orthogonal arrays and factor screening, structured fatigue testing can obtain more decision value with a limited number of experiments compared to an unplanned sequence of isolated experiments.

In aluminium fatigue research, methodology-focused studies show the value of well-planned experimental matrices. A careful test design helps researchers interpret fatigue behaviour more efficiently and with stronger statistical support [16]. At the same time, recent work on AA2024 points to a growing interest in combining physical insight with regression, numerical simulation, and data-driven modelling. These approaches describe fatigue performance in a more compact and accurate way [17, 18]. Together, these developments strengthen a clear point: modern fatigue studies should do more than report fatigue lives. They should also measure how each factor influences performance, so the results support practical engineering decisions.

The present study addresses this gap in metallurgical knowledge and design-ready fatigue assessment. A structured experimental matrix has been used for the study of the effect of stress amplitude and loading frequency on the fatigue life of AA2024 alloy for two different tempers. This is a framing that is essential for two reasons. Firstly, it clarifies whether the same alloy in two different metallurgical conditions has the same sensitivity to the changes of stress and frequency. Second, it enables the study to go past merely stating that one condition works better than another. Rather, the work can describe the effect of stress variation on fatigue life in the presence of frequency variation; how much additional effect does frequency variation have; and whether the difference between the effects of both variations is uniform over the given loading window. For fatigue-critical applications where the selected temper condition may have an impact on static qualification as well as acceptable stress margins, maintenance schedules, and durability, such a comparison is especially significant. The use of a design that is statistically structured is therefore not coincidental. A Repeated Stress-Frequency (RSF) design is a practical approach to investigating the main effects and relative magnitudes of stress-frequency combinations and conditions of materials. The advantages of these analysis tools are that they take fatigue data, and turn it into ranked engineering insight in this context – Taguchi-type orthogonal arrays, analysis of means and variance-based interpretation are appealing analysis tools. This approach does not lead to an overly large number of tests, but rather a well-structured (but complete) exploration of the design space. This is particularly important for AA2024, for which the fatigue behaviour is known to be a function of both microstructure and loading path.

In this context, the primary aim of the present study is to build a clear comparative understanding of the fatigue life of AA2024 alloy for two temper conditions, for varying stress amplitude and loading frequency in a controlled manner. Specifically, the study aims to: (i) produce a fatigue-life database for a specified stress-frequency range for both tempers; (ii) assess if the stress amplitude is the dominant parameter in fatigue life, as compared to the loading frequency; (iii) determine if one temper condition systematically delivers better fatigue life over the range studied; and (iv) translate the experimental observations into a statistically meaningful set of guidelines for fatigue-life-oriented material selection. The work is thus an important contribution to the fatigue design of the AA2024 alloy, using an experimentally controlled test plan and factor-ranking analysis. The research work is presented as a flowchart in Figure 1.

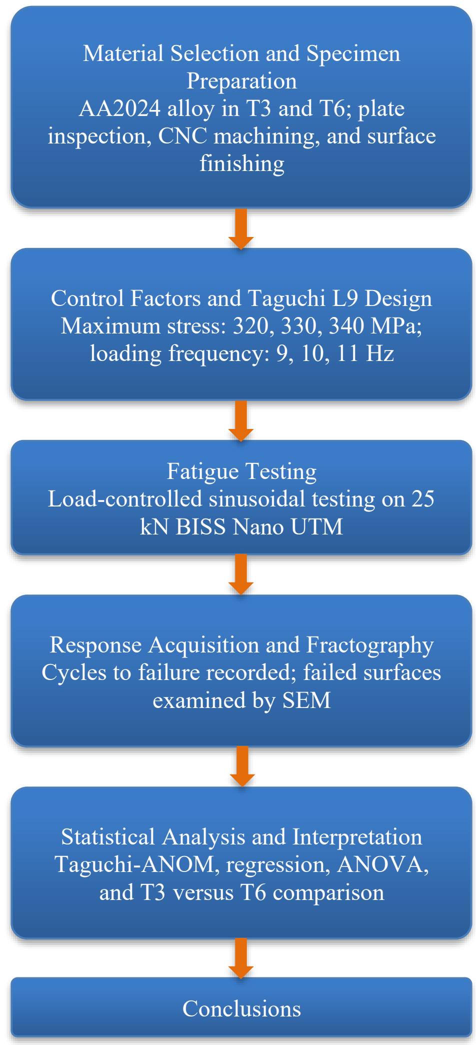

Fig. 1 Flowchart of the research work

2. Materials and Methods

2.1. Material and Temper Conditions

The material studied in this research is a commercial Al-Cu-Mg alloy (AA2024) in two heat-treated conditions, T3 and T6. The alloy has been solution treated, cold worked, and naturally aged in the T3 condition, giving the alloy a relatively coarse *S/θ′* precipitate microstructure and moderate dislocation density. T6 condition is a solution heat treatment and artificial ageing process which results in a more refined and compact distribution of strengthening precipitates for higher yield and ultimate tensile strength. Fatigue specimens were cut along the loading axis parallel to the rolling direction to represent typical aerospace use. The chemical composition of the material is mentioned in Table 1.

Table 1. Chemical composition of AA2024 (wt%) [19]

Cr	Cu	Fe	Mg	Mn	Si	Ti	Zn	Al
0.10	4.1	0.50	1.4	0.6	0.50	0.15	0.25	Bal

The plates were inspected visually first before extraction of the specimens in order to exclude areas with visible laps, deep scratchings and other macroscopic defects. In order to eliminate any influence of geometric and surface-condition artefacts on the differences in fatigue response and isolate it to the heat treatment, all subsequent machining, surface preparation and testing procedures were carried out in a similar manner for the two tempers.

2.2. Specimen Geometry and Surface Preparation

Figure 2 shows the geometry of the specimen that was chosen for fatigue testing according to ASTM E466 standard. To minimise geometric scatter, the plates were cut to make axisymmetric, hourglass-type fatigue specimens with a CNC lathe. The diameter and length of the gauge section were chosen in accordance with standard practice in uniaxial fatigue testing of wrought aluminium alloys, to provide a nominally uniform axial stress state in the central portion of the specimen, while minimising the risk of premature failure at the fillet transitions. Final diameters were held to within ±0.01 mm, and shoulder geometry had to be designed so that no bending moments were induced when the specimens were gripped in the testing machine.

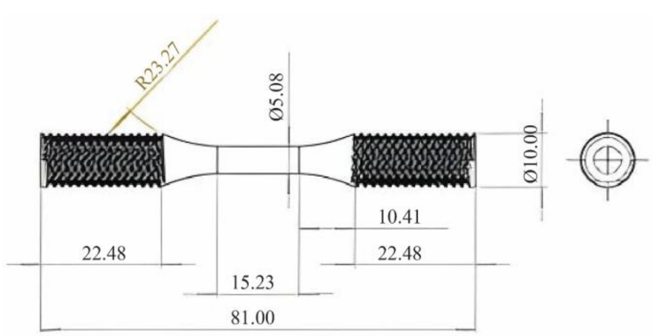

Fig. 2 Specimen configuration undertaken for fatigue testing

After machining, the gauge section of each specimen was progressively ground to a fine grit using SiC emery papers and then polished to a smooth surface that resembled a machined surface for typical aerospace components. This method minimized surface roughness-induced stress concentrations and minimized scatter from surface micro-notches. They were then degreased in acetone and air-dried for testing. The measured fatigue lives were predominantly representative of the intrinsic behaviour of the bulk microstructure in each temper, as there was no shot peening, coating or other surface treatment applied. The specimens post-fabrication can be seen in Figure 3.

Fig. 3 Fatigue specimens as per ASTM E466 standard, (a) AA2024-T3, (b) AA2024-T6

2.3. Experimental Design and Control Factors

The experimental fatigue test runs were designed using the Taguchi design-of-experiments approach to efficiently explore the combined effects of maximum stress level and loading frequency for each temper. Two control factors were considered:

- S (maximum stress level): 320, 330 and 340 MPa
- F (loading frequency): 9, 10 and 11 Hz

These levels were designed such that there were nine different stress-frequency combinations using an L_9 (3^2) orthogonal array. A 3 × 3 × 2 design space was created by L9 independently for AA2024-T3 and AA2024-T6. The fatigue life, for each combination, was taken as the number of cycles to the complete gauge section separation, or to a sudden drop in load associated with macroscopic crack growth.

The stresses selected were within the high-cycle range (between 10^4 and 10^5 cycles to failure) but not beyond the monotonic yield strength. The frequency range selected (9-11 Hz) was representative of the cyclic conditions to which aircraft components such as fuselage skins, wings, landing gear and control surfaces are subjected to, during service [20].

2.4. Fatigue Testing Procedure

Fatigue tests were conducted on a 25 kN Nano UTM of BISS make, which can work in stress-controlled mode. The machine is a servo-controlled universal testing system with an axial load frame and digital controller for constant-amplitude fatigue testing. Tests were conducted in laboratory air at room temperature, and a sinusoidal waveform was employed. The stress ratio was fixed at $R = \sigma_{min}/\sigma_{max} = 0$, i.e. fully pulsating tension with zero minimum stress. Specimens were mounted using appropriate grips, and alignment was carefully adjusted so that bending stresses are quasi-zero. In the first few cycles, the output of the machine was prudently checked to ensure that the signals were stable and had the desired amplitude and frequency. A minimum of two identical specimens was tested for each stress-frequency combination and temper.

The fatigue life values listed are the mean of all the replicate tests performed for each matrix point. Visual inspection of the test specimens was conducted after the test, and confirmed that there was good alignment with the fracture always occurring in the gauge section and not at the grips or fillets, thus confirming specimen quality.

2.5. Taguchi-ANOM Analysis

The response variable was the fatigue life, measured in terms of the number of cycles to specimen failure, N_f. The mean fatigue lives for the nine values in the L9 array were tabulated for each temper as a function of stress level and loading frequency.

A Taguchi Analysis of Means (ANOM) was used to compute the main effects of the two control factors and rank their relative importance. For a given temperature, the mean fatigue life at each level of a factor was obtained by averaging the means. N_f values across all tests sharing that level, irrespective of the other factor.

The "delta" of a factor was defined as the difference between its maximum and minimum level means. The dominant (Rank 1) factor had the greater delta, and the other factor was the secondary (Rank 2). These main-effects plots and ANOM tables offer a convenient graphical representation of the effect of stress amplitude and frequency changes on mean fatigue life for each temper.

2.6. Regression Analysis

Empirical fatigue-life prediction models of AA2024-T3 and AA2024-T6 were obtained by regression analysis, with maximum stress and loading frequency as variables. The fatigue life, L, was defined as the dependent variable, whereas the maximum stress level, S, and loading frequency, F, were defined as the independent variables.

A second-order polynomial model was chosen because it is possible that the two factors interact, each having a linear and quadratic relationship. Regressions were formulated separately for the different temper conditions because of the difference in metallurgical response.

In this study, the general regression model is given by the following equation: $L = \beta_0 + \beta_1 S + \beta_2 F + \beta_3 S^2 + \beta_4 F^2 + \beta_5 SF,$ where β_0 is the intercept, and β_1 to β_5 are regression coefficients.

2.7. Reproducibility and Uncertainty Considerations

A number of measures were implemented to improve the repeatability of the test campaign. All specimens were manufactured on the same CNC lathe and treated with the same grinding/ polishing procedure. The UTM was calibrated according to the standard procedures before the campaign, and test settings (maximum stress, frequency, R-ratio) were held constant for a given condition.

A minimum of two replicates per stress-frequency-temper combination minimized the influence of any unusual specimens within the replicate and allowed the reported mean lives to be interpreted as representative of the underlying condition. However, residual scatter in fatigue life was expected owing to microstructural heterogeneity, slight differences in surface finish and the stochastic nature of crack initiation at inclusions or second phase particles.

3. Results and Discussion

3.1. Overview of Fatigue Response of AA2024-T6 and AA2024-T3

Summary of the fatigue lives measured experimentally for AA2024 in the T6 and T3 tempers, tested at the three stress amplitudes (320, 330 and 340 MPa) and loading frequencies (9, 10 and 11 Hz) are given in Table 2. As an example, typical specimens (highest and lowest fatigue life scenarios) post fatigue failure are shown in Figure 4.

(a)

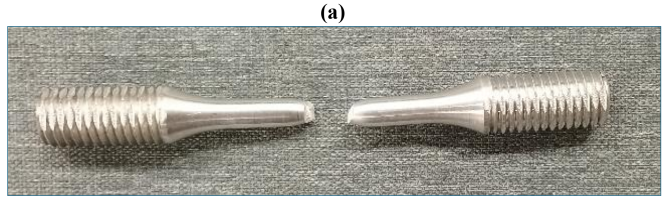

(b)

Fig. 4 Specimens with the highest and lowest fatigue lives, (a) Run 1 of AA2024-T3 at 320 MPa & 9 Hz, (b) Run 9 of AA2024-T6 at 340 MPa & 11 Hz

In all test conditions, the S-N response followed the expected monotonic relationship, that is, increasing the maximum stress level from 320 to 340 MPa decreases the fatigue life for the tempers.

For AA2024-T6, the fatigue life decreased from about 4.30×10^4 cycles at 320 MPa to 2.40×10^4 cycles at 340 MPa, leading to a reduction of about 44%. A similar but slightly less severe drop of about 39% was observed in AA2024-T3, with the fatigue life reducing from about 4.66×10^4 to 2.82×10^4 cycles over the same stress range.

Table 2. Fatigue results of AA2024-T6 and AA2024-T3

Run	Max. Stress Level (MPa)	Loading Freq. (Hz)	Fatigue Life (cycles)	
			AA2024-T6	AA2024 -T3
1	320	9	44732	48769
2	320	10	42547	45997
3	320	11	41683	44892
4	330	9	36562	42175
5	330	10	33989	38994
6	330	11	32396	36889
7	340	9	24861	29321
8	340	10	23964	28213
9	340	11	23100	26929

This major stress effect is followed by a secondary effect of loading frequency. The fatigue life decreased as the frequency increased from 9 to 11 Hz, but the reduction was not that big when compared to the stress amplitude. The frequency sensitivity for AA2024-T6 is approximately 8-9% within the 9-11 Hz range, and for AA2024-T3 was slightly higher at around 9-10%. The results of the above observations suggest that the fatigue response in the studied regime was strongly dependent on the amplitude of the applied stress, and the frequency played a secondary role in the initiation of the crack and the growth of the short crack. Importantly, AA2024-T3 always performed better than AA2024-T6 under all stress/frequency combinations. The improvement in fatigue life was between 7-9% at the lowest stress level (320 MPa) and almost 18% at the highest stress level (340 MPa), with an average of about 13-14% for the design space. This systematic advantage implies that, despite the T6 temper being generally the more suitable one for high static strength, the T3 temper seems to be the more favourable one for high cycling fatigue under the present loading conditions.

3.2. Fractographic Interpretation of Fatigue Damage Evolution in AA2024-T6 and AA2024-T3

Under the selected loading conditions, the SEM fractographs show that the fatigue damage evolution is significantly different for AA2024-T3 and AA2024-T6. For the case of Run 1 of AA2024-T3 at 320 MPa and 9 Hz, the fracture surface in Figure 5(a) had a relatively wider region of crack propagation followed by a gradual transition to final rupture. This shows a lower rate of crack growth and a longer stage of fatigue damage accumulation, and confirms the better fatigue life of the T3 temper. The surface morphology indicates that the failure is dominated by stable fatigue propagation before final fracture.

The most extreme loading condition in the present matrix, as shown in Figure 5(b), is Run 9 of AA2024-T6 at 340 MPa and 11 Hz, and is expected to have the smallest stable crack-growth region and the largest final fracture zone. Under this condition, the fracture surface features rapid crack propagation and abrupt final failure because of the significant decrease in the fatigue life at the higher stress and frequency. The cyclic damage localization behaviour seen in this is more sensitive to severe loading conditions in the T6 condition, resulting in faster crack coalescence and quicker overload failure.

Overall, the fractographic comparison has confirmed that the fatigue damage of AA2024-T3 was a more gradual process than AA2024-T6 under higher stress-frequency conditions. The observations are in good agreement with the fatigue-life results and uphold the determination that the T3 temper is more resistant to fatigue crack evolution in the range of loading investigated.

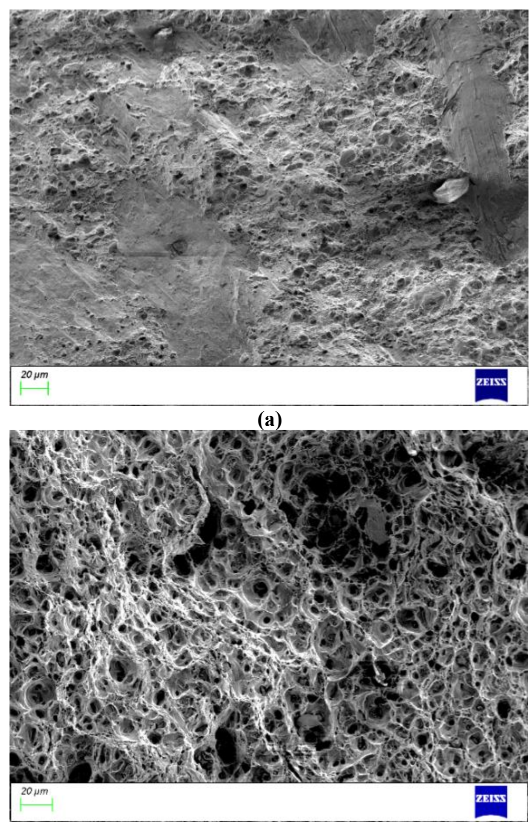

(a)

(b)

Fig. 5 SEM images of the highest and lowest FL scenarios, (a) Run 1 of AA2024-T3 at 320 MPa & 9 Hz, (b) Run 9 of AA2024-T6 at 340 MPa & 11 Hz

3.3. Taguchi Analysis

An analysis of means was carried out on the fatigue life data for each temper to quantify the relative influence of the stress level and loading frequency. Figures 6 and 7 represent the main-effects plots, and Tables 3 and 4 are ranked factor statistics, which give a succinct representation of the effect that each control factor has on the mean response.

For AA2024-T6, the mean fatigue lives at 320, 330 and 340 MPa are approximately 4.30×10^4, 3.43×10^4 and 2.40×10^4 cycles, respectively. The corresponding ANOM for the stress factor ($\approx1.90\times10^4$ cycles) is one order of magnitude greater than that for loading frequency ($\approx3.0\times10^3$ cycles) and clearly indicates that stress amplitude is the most significant factor (Rank 1) and loading frequency is of secondary importance (Rank 2).

An analogous trend is obtained for AA2024-T3: the mean lives at 320, 330 and 340 MPa are $\approx4.66\times10^4$, 3.94×10^4 and 2.82×10^4 cycles, with a stress-related delta of $\approx1.84\times10^4$ cycles compared to $\approx3.85\times10^3$ cycles for frequency.

For both temperatures, the observed variation in fatigue life is governed predominantly by stress amplitude, while loading frequency acts as a secondary modifier. In other words, frequency fine-tunes the fatigue response, but it does not control the primary fatigue-life trend.

The ANOM plots also show that the fatigue life drops off almost linearly with the applied stress, and is less sensitive to frequency. The highest average life is seen at the lowest stress and lowest frequency (320 MPa, 9 Hz); at 340 MPa and 11 Hz is the worst-case performance for both T6 and T3. This is in line with classical fatigue theories that suggest that a higher number of cycles increases the rate of crack nucleation at inclusions, second phase particles or persistent slip bands, and that an increase in cyclic frequency shortens the relaxation time of local stresses and microstructural recovery per cycle.

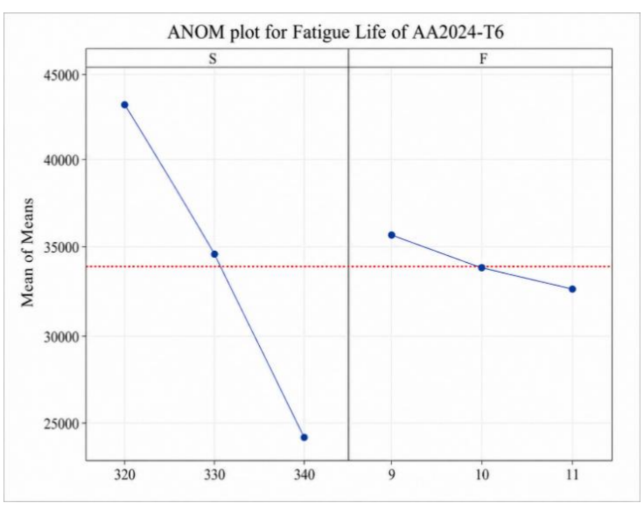

Fig. 6 ANOM plot for fatigue life of AA2024-T6

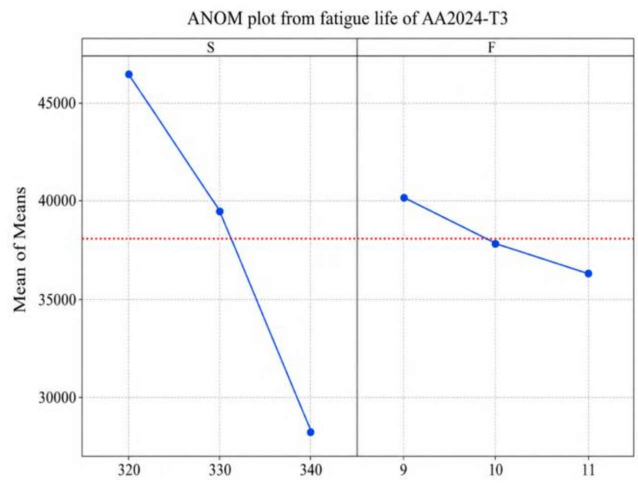

Fig. 7 ANOM plot for fatigue life of AA2024-T3

Table 3. ANOM rankings of factors for fatigue life of AA2024-T6

Level	S	F
1	42987	35385
2	34316	33500
3	23975	32393
Delta	19012	2992
Rank	1	2

Table 4. ANOM rankings of factors for fatigue life of AA2024-T3

Level	S	F
1	46553	40088
2	39353	37735
3	28154	36237
Delta	18398	3852
Rank	1	2

3.4. Comparative Fatigue Performance of T3 versus T6

One of the major findings in this study is the significant superiority of AA2024-T3 over AA2024-T6 for fatigue life in the entire stress and frequency matrix. The T3 temper offers from around 7% to 18% longer life at each test point compared to T6, and is more significant at higher stress levels. For example, at 340 MPa and 9 Hz, the fatigue life improves from 2.49×10^4 (T6) to 2.93×10^4 cycles (T3), i.e. nearly an 18% gain. The trend is not as intuitive as it might seem when only static strength is taken into account: a condition of artificial ageing (T6) is typically aimed at maximizing yield and ultimate strength by achieving a dense distribution of strengthening precipitates, while a condition of natural ageing (T3) after the cold work often has lower tensile strength. However, the subtle balance between strength, cyclic slip behaviour, residual stresses and the stability of precipitate–matrix interface is the key factor that controls high-cycle fatigue. In the present case, the T3 microstructure may provide a more uniform slip distribution and may retard the initiation of microcrack coalescence, which may lead to an even greater increase in fatigue life when compared to the slightly reduced static properties.

Design-wise, this outcome can mean that the AA2024-T3 is a competitive or even better material than AA2024-T6 for components to which fatigue performance under moderate stress amplitudes and service-relevant frequencies is important. This minor but steady life extension can be used to raise the allowable stress, given the desired life, or to give more safety margins while maintaining the geometric design.

3.5. Interaction of Stress Amplitude and Frequency

Taguchi analysis identified stress as the dominant factor; the frequency effect is not negligible, particularly when both factors are at their most severe levels. At 320 MPa, increasing frequency from 9 to 11 Hz produces only a slight reduction in life for both tempers, but at 340 MPa, the same frequency shift resulted in a more critical synergy between the two variables. In practical terms, this means that the penalty associated with operating at higher frequencies becomes more severe as the applied stress approaches the yield point. For structures subjected to variable-amplitude and variable-frequency loading (e.g., rotating machinery with speed ramps, aerospace control surfaces under gust loading), the combined effect of elevated stress and high frequency should therefore be carefully considered in damage tolerance assessments. The present dataset provides a first quantitative indication of how quickly life can deteriorate when both factors drift towards their unfavourable ends.

3.6. Regression Analysis and ANOVA

The regression equations for AA2024-T6 and AA2024-T3 (Table 5) had R^2 values of 0.9979 and 0.9966, respectively, which means that over 99% of the variance of the fatigue life was captured by the linear and quadratic terms and interactions between maximum stress and loading frequency. The regression coefficients are meaningful and are consistent with the Taguchi and ANOM results. In both temperatures, positive linear stress term and negative quadratic stress term give rise to concave down dependence of life on stress, indicating that the fatigue durability of the material decreases rapidly with the increase in the applied stress. The other terms of the frequency are smaller, indicating that the frequency is a secondary factor, but not negligible.

Table 5. Regression equations along with R^2 values for both temperatures

Temper	Regression Equation	R^2
T6	$L = -400890.67 + 4235.08S - 19902.00F - 8.345S^2 + 389.00F^2 + 32.20S\times F$	0.9979
T3	$L = -1649898.39 + 11903.33S - 22733.75F - 19.99S^2 + 427.83F^2 + 37.13S\times F$	0.9966

Table 6, ANOVA for AA2024-T6, shows that the factor S is clearly the largest factor, contributing some 97% of the total sum of squares, while the factor F contributes just 2.4%. The quadratic terms (S^2 and F^2) and the interaction term (S×F) are not significant. This shows that the fatigue life of the T6 temper is almost exclusively dependent on the applied stress, and the correction factors from frequency of operation and other higher-order factors are small. Table 7, ANOVA for AA2024-T3, also identifies S as the primary driver of fatigue life (93.9% contribution), but with a slightly higher influence of F (4.1%) and a modest increase in the contributions from S^2 and the interaction term. This suggests a mildly more curved and coupled response surface for T3 than for T6, which is consistent with the stronger frequency sensitivity inferred from the Taguchi and regression analyses. This also confirms that stress amplitude is the principal driving factor for enhancing fatigue life in both tempers.

Table 6. ANOVA for the results of AA2024-T6

Source	DF	SS	MS	% Contribution
S	1	542203228	542203228	97.01
F	1	13428096	13428096	2.40
S^2	1	1392780	1392780	0.25
F^2	1	302642	302642	0.05
S×F	1	414736	414736	0.07
Error	3	1182153	394051	--
Total	8	558923636	--	--

Table 7. ANOVA for the results of AA2024-T3

Source	DF	SS	MS	% Contribution
S	1	507748004	507748004	93.90
F	1	22253004	22253004	4.12
S^2	1	7993335	7993335	1.48
F^2	1	366083	366083	0.07
S×F	1	551306	551306	0.10
Error	3	1838175	612725	--
Total	8	540749907	--	--

3.7. Confirmation Testing and Validation of Regression Predictions

Robustness of the regression models was verified by the confirmation experiments carried out in the intermediate stress-frequency conditions, different from the L9 matrix. The fatigue life predicted, and experimental results were compared and found to be close, as shown in Table 8, for both tempers with a deviation of 5.07%-7.02%. For AA2024-T6, the deviations were 5.56% and 7.02%, while for AA2024-T3, they were 5.07% and 6.13%.

It was found that all the errors were less than 10%, indicating acceptable predictive accuracy of the regression equations developed. The expected physical trend (in terms of fatigue life) was also maintained, with AA2024-T3 having superior fatigue life than AA2024-T6 under similar loading conditions. Hence, the regression models are deemed as valid for preliminary fatigue-life estimation for the range of stress and frequency levels examined.

Table 8. Fatigue results from regression and confirmation experiments

S.No	Temper	S (MPa)	F (Hz)	Fatigue Life (cycles)		% Deviation
				Regression	Experiment	
1	T6	325	9	40646	38504	5.56
2	T6	335	10	29094	27186	7.02
3	T3	325	9	45896	43683	5.07
4	T3	335	10	34170	32195	6.13

4. Conclusion

The fatigue test performance of AA2024 alloy in T3 and T6 temper was systematically investigated with the maximum stress and loading frequency varied by using Taguchi L9 experimental design. The results showed that the primary factor affecting fatigue life is the stress amplitude, and that frequency of loading has a secondary but measurable effect. Experimental, statistical, regression, and fractographic analyses resulted in AA2024-T3 being the more fatigue-resistant material for the loading window investigated. The key findings are summarized below:

- Increasing the maximum stress from 320 to 340 MPa reduced the average fatigue life of AA2024-T6 by approximately 44%, from about 4.30×10^4 to 2.40×10^4 cycles.
- Under the same stress increase, the average fatigue life of AA2024-T3 decreased by approximately 39%, from about 4.66×10^4 to 2.82×10^4 cycles.
- AA2024-T3 consistently outperformed AA2024-T6 across all tested stress-frequency combinations, giving a fatigue-life improvement of approximately 7-18%.
- Taguchi-ANOM and ANOVA confirmed that stress amplitude was the dominant factor controlling fatigue life. Its contribution was 97.01% for AA2024-T6 and 93.90% for AA2024-T3.
- Loading frequency had a smaller but noticeable effect, contributing 2.40% for AA2024-T6 and 4.12% for AA2024-T3.
- SEM fractography supported the fatigue-life results. AA2024-T3 showed evidence of more gradual fatigue damage evolution, whereas AA2024-T6 exhibited features associated with faster crack propagation and earlier final failure under severe loading.
- The regression models showed excellent agreement with the experimental data, with $R^2 = 0.9979$ for AA2024-T6 and $R^2 = 0.9966$ for AA2024-T3.
- Confirmation tests validated the regression models, with prediction deviations ranging from 5.07% to 7.02%, confirming acceptable predictive accuracy within the investigated stress-frequency range.

The results indicate that AA2024-T3 is more resistant to fatigue than AA2024-T6 in the range of the investigated high-cycle fatigue regime. Extension of the present work to encompass a larger range of stress ratios, a wider spectrum of frequencies, variable amplitude loading, environmental exposure, and detailed microstructural quantification is recommended to enable translation of the present findings into more service-representative fatigue-life prediction models.

Acknowledgments

The authors would like to thank the managements of Vidya Jyothi Institute of Technology, KG Reddy College of Engineering and Technology, and Vasavi College of Engineering, for their support and encouragement in successfully executing this collaborative research.

References

[1] E.A. Starke, and J.T. Staley, "Application of Modern Aluminum Alloys to Aircraft," *Progress in Aerospace Sciences*, vol. 32, no. 2-3, pp. 131-172, 1996. [CrossRef] [Google Scholar] [Publisher Link]

[2] A. Heinz et al., "Recent Development in Aluminium Alloys for Aerospace Applications," *Materials Science and Engineering A*, vol. 280, no. 1, pp. 102-107, 2000. [CrossRef] [Google Scholar] [Publisher Link]

[3] P. Rambabu et al., *Aluminium Alloys for Aerospace Applications*, Aerospace Materials and Material Technologies, pp. 29-52, 2016. [CrossRef] [Google Scholar] [Publisher Link]

[4] Shuang-Shuang Li et al., "Development and Applications of Aluminum Alloys for Aerospace Industry," *Journal of Materials Research and Technology*, vol. 27, pp. 944-983, 2023. [CrossRef] [Google Scholar] [Publisher Link]

[5] Abdelghani Mokdad et al., "Cyclic behavior of AA2024 Aluminum Alloy Under Different Loading Paths and Heat Treatments," *Fatigue & Fracture of Engineering Materials & Structures*, vol. 47, no. 3, pp. 677-688, 2024. [CrossRef] [Google Scholar] [Publisher Link]

[6] Aymen Khadimallah et al., "Characterization of Fatigue Behavior of AA2024-T351 Aluminum Alloy," *Fatigue & Fracture of Engineering Materials & Structures*, vol. 46, no. 10, pp. 3729-3744, 2023. [CrossRef] [Google Scholar] [Publisher Link]

[7] S. Khan, O. Kintzel, and J. Mosler, "Experimental and Numerical Lifetime Assessment of Al 2024 Sheet," *International Journal of Fatigue*, vol. 37, pp. 112-122, 2012. [CrossRef] [Google Scholar] [Publisher Link]

[8] S. Khan et al., "Low Cycle Fatigue Damage Mechanism of the Lightweight Alloy Al2024," *International Journal of Fatigue*, vol. 38, pp. 92-99, 2012. [CrossRef] [Google Scholar] [Publisher Link]

[9] M. F. Borges et al., "Fatigue Crack Propagation Analysis in 2024-T351 Aluminium Alloy Using Nonlinear Parameters," *International Journal of Fatigue*, vol. 153, pp. 1-10, 2021. [CrossRef] [Google Scholar] [Publisher Link]

[10] Qi Zhao et al., "Fatigue Crack Propagation of AA2024 Alloy Under Texture Control Using Crystal Plasticity Coupled with Accelerated Cyclic Cohesive Zone Model," *Engineering Fracture Mechanics*, vol. 296, 2024. [CrossRef] [Google Scholar] [Publisher Link]

[11] M. Krkoska et al., "Fatigue Crack Paths in AA2024-T3 When Loaded with Constant Amplitude and Simple Underload Spectra," *Engineering Fracture Mechanics*, vol. 77, no. 11, pp. 1857-1865, 2010. [CrossRef] [Google Scholar] [Publisher Link]

[12] Xiaoting Liu et al., "Experimental Study of the Fatigue Failure Behavior of Aluminum Alloy 2024-T351 under Multiaxial Loading," *Engineering Failure Analysis*, vol. 164, 2024. [CrossRef] [Google Scholar] [Publisher Link]

[13] H. Mayer, R. Schuller, and M. Fitzka, "Fatigue of 2024-T351 Aluminium Alloy at Different Load Ratios up to 10^{10} Cycles," *International Journal of Fatigue*, vol. 57, pp. 113-119, 2013. [CrossRef] [Google Scholar] [Publisher Link]

[14] Jose I. Rojas, and Daniel Crespo, "Onset Frequency of Fatigue Effects in Pure Aluminum and 7075 (AlZnMg) and 2024 (AlCuMg) Alloys," *Metals*, vol. 6, no. 3, pp. 1-12, 2016. [CrossRef] [Google Scholar] [Publisher Link]

[15] Ruslan Kuliiev et al., "On the Effect of Testing Frequency on High and Very High Cycle Fatigue Behavior of AA2024-T3, Ti-6Al-4V, and Inconel 718," *Journal of Materials Engineering and Performance*, vol. 32, pp. 10843-10856, 2023. [CrossRef] [Google Scholar] [Publisher Link]

[16] S. Martin-Béjar et al., "Experimental Methodology Design for Fatigue Behaviour Analysis of Turned Aluminum Alloys," *Procedia Manufacturing*, vol. 13, pp. 73-80, 2017. [CrossRef] [Google Scholar] [Publisher Link]

[17] Shahan Mazlan et al., "Experimental and Numerical Analysis of Fatigue Life of Aluminum Al 2024-T351 at Elevated Temperature," *Metals*, vol. 10, no. 12, pp. 1-14, 2020. [CrossRef] [Google Scholar] [Publisher Link]

[18] Zhaoji Li,Haitao Yue et al., "Fatigue Life Prediction of 2024-T3 Al Alloy by Integrating Particle Swarm Optimization-Extreme Gradient Boosting and Physical Model," *Materials*, vol. 17, no. 21, pp. 1-22, 2024. [CrossRef] [Google Scholar] [Publisher Link]

[19] Jagadesh Kumar Jatavallabhula et al., "Development and Assessment of Machine Learning Models for Predicting Fatigue Response in AA2024," *Materials Research Express*, vol. 12, no. 1, pp. 1-19, 2025. [CrossRef] [Google Scholar] [Publisher Link]

[20] Daqian Zhang, and Yueyang Chen, "Random Vibration Fatigue Life Analysis of Airborne Electrical Control Box," *Applied Sciences*, vol. 12, no. 14, pp. 1-19, 2022. [CrossRef] [Google Scholar] [Publisher Link]